THE ASTROPHYSICAL JOURNAL, 558:L137–L140, 2001 September 10

OBSERVATION OF THE CORONAL HARD X-RAY SOURCES OF THE 1998 APRIL 23 FLARE

J. SATO[1]
NASA Goddard Space Flight Center, Code 682, Greenbelt, MD 20771; sato@solar.isas.ac.jp
Received 2001 May 29; accepted 2001 August 2; published 2001 August 15

ABSTRACT

We analyzed Hard X-Ray Telescope observations of an X1.2 flare on 1998 April 23. This flare is one of the best examples for studying coronal hard X-ray sources due to the intensity of the emission and the occultation of the footpoints. In this flare, coronal hard X-ray sources composed of both thermal and nonthermal emissions showed complex structure unlike any previously observed. Dominant thermal and nonthermal sources do not come from the same loop-top region. Nonthermal sources include two sources in the low corona ($\sim 2.7 \times 10^3$ km) and an extended source in the high corona ($\sim 5 \times 10^4$ km). These observations of nonthermal coronal sources suggest that energetic phenomena occur in the low corona at first, and energized electrons are then injected into a high coronal region.

Subject headings: plasmas — Sun: flares — Sun: X-rays, gamma rays

1. INTRODUCTION

A solar flare is one of the most energetic phenomena in the solar corona. Enormous energy is released, and electrons are accelerated to high energies. Since these electrons are produced in the corona, the study of coronal hard X-ray emission is one of the most important keys to understanding the production of high-energy electrons. The finding of a high-energy hard X-ray source located above the soft X-ray loop, the so-called Masuda source (Masuda et al. 1995), is one of the most important results obtained with the Hard X-Ray Telescope (HXT; Kosugi et al. 1991; Sato, Kosugi, & Makishima 1999) on board the *Yohkoh* satellite. Various studies of this source have been done from both the observational and theoretical viewpoints (e.g., Alexander & Metcalf 1997). Some authors conclude that the Masuda source has nonthermal spectral characteristics although the image quality and spectral resolution are not high.

Since high-quality imaging requires sufficient photon counts and the coronal hard X-ray source in the higher energy range is typically weak compared with the footpoint emission, one of the best ways to study strong coronal emission is to study an intense flare with the footpoints occulted by the solar limb. The 1998 April 23 flare is just such a case. Also, this event is suitable for studying large coronal structures since it shows a large soft X-ray arcade. Using the spatially integrated hard X-ray and radio fluxes measured with HXT and the Nobeyama Radio Heliograph, Sato & Hanaoka (2000) showed that the hard X-ray emission is from a mixture of thermal electrons with a temperature of ~30 MK and nonthermal electrons ($\lesssim$100 keV) with a hard spectrum and that radio emission is due to gyrosynchrotron from nonthermal electrons (on the order of ~1 MeV). These images do not necessarily agree with each other. A strong hard X-ray source (33–53 keV) observed in the impulsive phase is located above the radio 17 GHz source existing around the top of the soft X-ray arcade. However, the X-ray and radio images show two similarities, i.e., a source motion along the top of the soft X-ray arcade and an increase in the size near the peak time. These similarities suggest that the radio and hard X-rays are from energetic electrons with the same origin.

In this Letter, based on hard X-ray images over the four HXT energy bands, we reveal a spatial relation between thermal and nonthermal emissions and study the nonthermal sources in detail.

2. FLARE EMISSION AND HARD X-RAY DATA ANALYSIS

The *GOES* class X1.2 flare occurred in NOAA Active Region 8210 on 1998 April 23. The soft X-ray emission began at 05:35 UT and peaked at 06:23 UT. The longitude of the active region (NOAA AR 8210) at this time is estimated to be E103° by following the images (see Fig. 2) taken with the Soft X-Ray Telescope (SXT; Tsuneta et al. 1991) on board *Yohkoh*. This corresponds to an occultation height of $\sim 1.7 \times 10^4$ km.

The hard X-ray time profiles observed in the four HXT energy bands (L: 14–23 keV, M1: 23–33 keV, M2: 33–53 keV, H: 53–93 keV) and in the Hard X-Ray Spectrometer (HXS; Yoshimori et al. 1991; 102–174 keV in this Letter) are shown in Figure 1. Different time behaviors are evident in the lower and higher energy bands. In the lower energy bands (L and M1), the emission is mainly gradual, suggesting a thermal plasma. The time profile in the L band shows a slow increase of the intensity from the beginning to 05:38 UT followed by a more rapid increase to the peak and a gradual decrease after the peak. The emission in the M1 band is similar to that of the L band. In the higher energy bands (M2 and H), the emission shows a more spiky structure on the rise and at the peak until ~05:45 UT. Two distinct spikes are evident on the rise around 05:36:30 UT (labeled "a") and 05:38:30 UT ("c"). After that, in the H band, the emission has two gradual peaks with the same intensity around 05:41 UT ("e") and 05:43 UT ("g"). In the decay phase, the intensity decreases monotonically in all bands except for an enhancement at ~05:56 UT. In HXS, we observed high-energy photons above 100 keV with a time structure similar to that in the H band.

For the study of the morphological structure of the hard X-ray sources, eight intervals were selected as shown in Figure 1 (denoted as "a"–"h"). These intervals were selected to cover specific time profile structures, i.e., peaks and valleys. We could not analyze H-band images for the second enhancement at ~05:56 UT because of the low photon counts. We used the revised maximum entropy method algorithm and improved instrumental parameters developed by Sato et al. (1999) to synthesize HXT images.

[1] Present address: Physics Department, Montana State University, P.O. Box 173840, Bozeman, MT 59717.

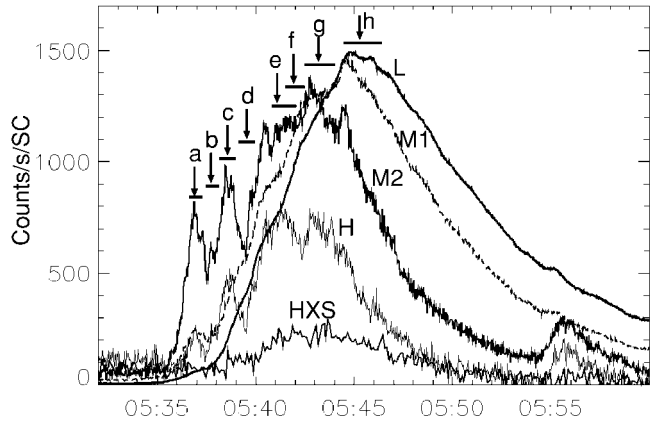

FIG. 1.—Hard X-ray time profiles observed with HXT multiplied by the following factors for clarity: L = 1, M1 = 7, M2 = 70, H = 90. HXS data is overlaid within the figure. Background rates are subtracted. Images in Figs. 2*a*–2*h* were taken at the times marked by the corresponding labeled arrows.

3. SPATIAL CHARACTERISTICS OF THE LOOP-TOP HARD X-RAY SOURCES

Figures 2*a*–2*h* show L and M2 hard X-ray images for the selected time intervals indicated in Figure 1. In the L band, at the beginning of hard X-rays (Fig. *a*), the brightest area is located in the south at the effective altitude of $\sim 2.4 \times 10^4$ km above the limb. Around 05:38 UT (Fig. 2*b*), during the abrupt increase in the intensity, a strong L-band source appears at lower altitude than the earlier bright region seen in Figure 2*a*. As time progresses, the bright area moves northward (Figs. 2*b*–2*g*). The averaged speed is about 40 km s^{-1}. Around the peak time in the L band, the images (Figs. 3*f*–3*h*) show an increase in height with a speed of about 10 km s. The M1-band images are similar to the L-band images shown here, as expected from the similar time profiles in these two energy bands.

In the M2 band, the source structure is more complicated. Images that correspond to the two spikes marked "a" and "c" in Figure 1 are shown in Figures 2*a* and 2*c*. In these figures, the brightest area is observed at almost the same position. This is called the S1 source, corresponding to an altitude of $\sim 2.7 \times 10^4$ km. However, images before and after these spikes, i.e., Figures 2*b* and 2*d*, show that the brightest source (denoted as "S2") is located at another place whose position is further to the north at almost the same altitude. The distance between these two sources is about 8×10^3 km on the plane of the sky.

Around the peak time (intervals e–g), the M2-band images show the most complicated structure. In Figure 2*e*, in the north region, the brightest source (denoted as "N") is observed consistent with the L-band source. In contrast, the S2 source increases in size and moves to a higher altitude. In Figure 2*f*, we clearly see two cusp structures, one above S2 and the other above N. Then, in Figure 2*g*, an extended structure (denoted as E) is clearly seen in the higher corona with an estimated altitude of $\sim 5 \times 10^4$ km. After the hard X-ray peak (Fig. 2*h*), the strong source (N) becomes the dominant source while the S2 source remains relatively weak.

Figure 3 shows the same M2-band image for interval g from Figure 2*g* together with the SXT image (Beryllium filter) at nearly the same peak time. These images are relatively coaligned within 0.″1. The SXT image shows a ridge of a soft X-ray arcade with an elongated structure above the limb. There is also very weak emission extended into the high corona with multiple cusps (*white dotted lines*). The south hard X-ray (S2) source is located above the bright elongated structure in soft X-rays. The north hard X-ray (N) source is almost cospatial with the brightest soft X-ray emission in this region. We clearly see extended hard X-ray emission from a higher region in the corona than the weakest visible soft X-ray emission.

4. THERMAL AND NONTHERMAL CHARACTERISTICS OF EACH REGION

In order to study the time behavior and spectral characteristics of the hard X-ray–emitting sources, we divided the images into three regions (see Fig. 2*g*): north (N), south (S1 + S2), and extended (E), based on the M2-band image. Since the L and M1 time profiles show only gradual variation, we assume that the emissions in these bands are thermal and calculate the electron temperature (Te) and emission measure (EM) using the fluxes in these two bands alone. We then calculate the photon counts expected in higher bands that would be obtained for a thermal

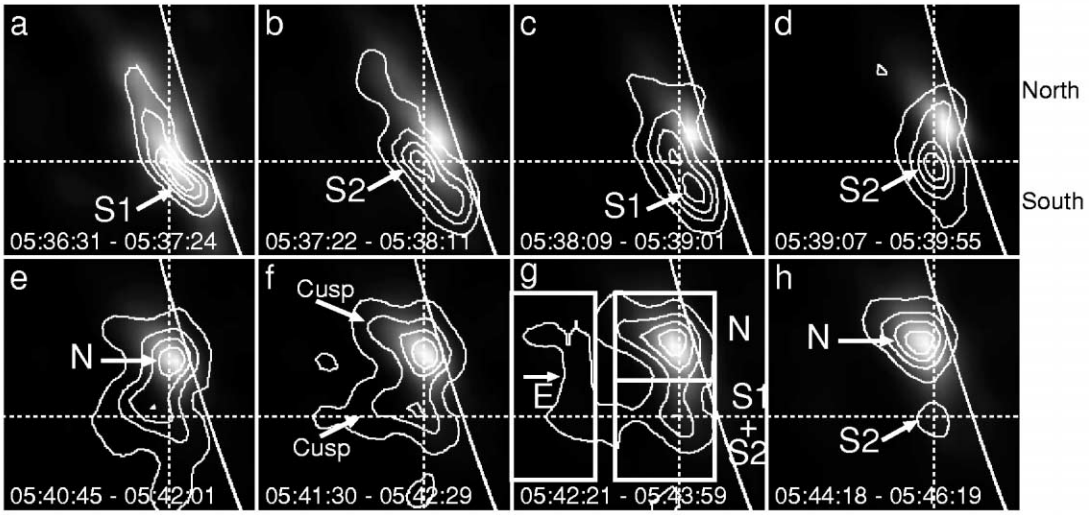

FIG. 2.—Evolution of hard X-ray images in the L band (*gray scale*) and M2 band (*contours*) from the start of the event to the time of the hard X-ray peak. The images are for the times indicated with the same letters in Fig. 1. The contour levels are at 20%, 40%, 60%, and 80% of the peak intensity within each map. The field of view is 78″ × 78″. Three hard X-ray sources observed in the M2 band in the low corona are labeled S1, S2, and N. An extended source in the high corona is labeled E. The three boxes shown in (*g*) are regions used to determine the fluxes plotted vs. time in Fig. 4.

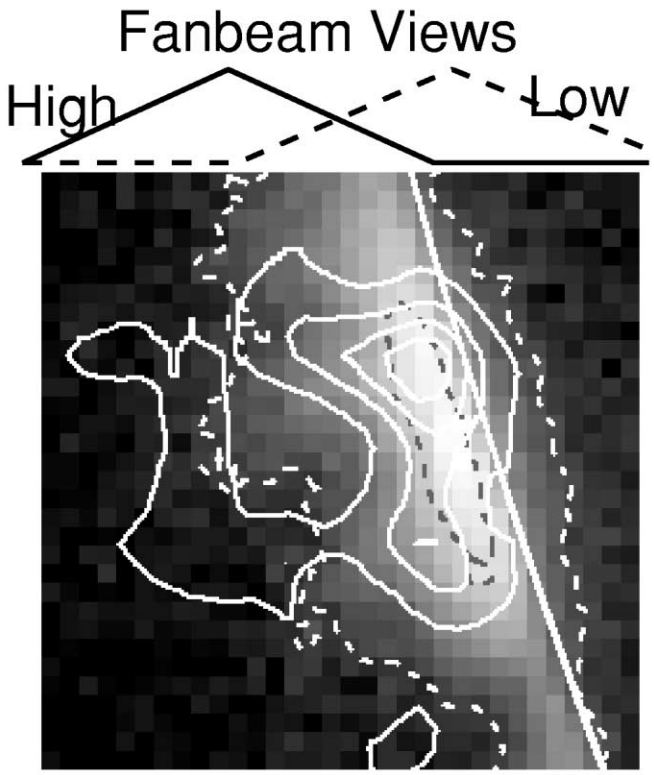

FIG. 3.—Comparison between SXT (Be) and HXT (M2) images near the peak time. The hard X-ray image (*thick white contour*) around the peak time is coaligned with an SXT image (*gray scale and dotted contours*). The SXT image was taken at 05:43:10. The dotted contours are at 60% and 2% of the maximum brightness. The HXT M2-band image is the same as that shown in Fig. 2*g*. Two fan-beam sensitivity patterns that extend in the north-south direction over the whole area are shown at the top of the figure.

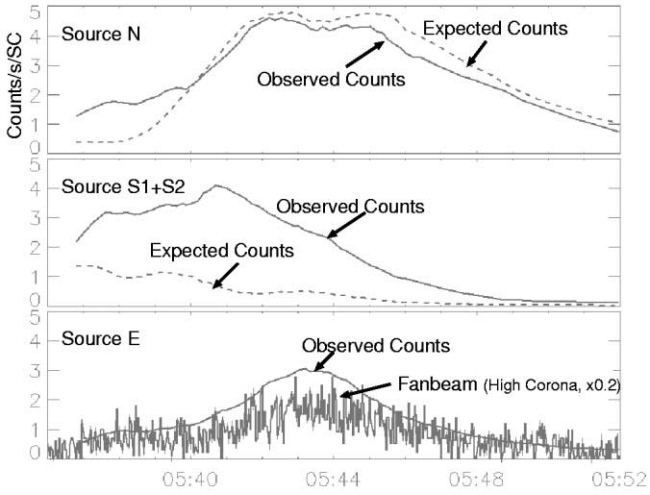

FIG. 4.—M2-band time profiles for three areas shown in Fig. 2*g*. The dotted lines show the M2-band count rate expected from thermal plasma with the Te and EM derived from the fluxes in the L and M1 bands. In region E, we plotted 2 s data derived from fan-beam elements observing the high corona (see Fig. 3). Note that a long time interval (~2 minutes) is adopted for the high-quality imaging, and therefore time profiles are boxcar-averaged with this smoothing time.

spectrum with these parameters. Figure 4 shows the boxcar average (120 s smoothing time) time profiles of the observed and expected photon count rate from the N and S1 + S2 regions in the M2 band. The extended source E is evident only in the M2 band, and therefore we cannot calculate an expected photon count rate for a thermal spectrum in the same way. Instead, we plotted fan-beam data (see below) observing the extended region.

The northern region (N) shows a gradual time profile with a similar source position over the soft X-ray and L–M2 bands. Also, the expected photon count rates in the M2 band agree well with observed photon count rates except near the beginning of the flare. Near the peak time at 05:44 UT, the temperature and EM derived from the low-energy bands are 34 MK and 9×10^{48} cm^{-3}, respectively.

In the southern region (S1 + S2), Figure 4 shows that the measured time profile is quite different from the expected one assuming a purely thermal source with a single temperature. The expected photon count rate from the thermal component is low, and the intensity decreases monotonically as time progresses. Also, the hard X-ray time profile observed with HXS is similar to that of the southern region during the impulsive phase (see Fig. 1). Therefore, we conclude that the south sources (S1 and S2) observed in the M2 band are mainly from nonthermal electrons.

In the extended region (E), the time profile derived from fan-beam data is noisy but it shows gradual time behavior consistent with the boxcar-averaged profile. The peak (interval g, ~05:44 UT) is delayed by ~2 minutes from the peak of the southern sources. The peak in the flux from the E region is almost at the same time as the peak at around 05:44 UT seen in the H band and HXS profiles. Also, in this region, we could not observe any L- and M1-band source corresponding to the M2 source. This means that we cannot expect sufficient photon counts from a thermal plasma to explain the M2-band image even if a thermal plasma existed at this location. These facts suggest that the extended structure observed in the M2 band is most likely to be a nonthermal source.

In order to clarify the characteristics of the coronal sources at different altitudes, we have used two of the HXT fan-beam elements. All HXT elements obtain spatial information of sources that is modulated in one dimension by the X-ray transmission pattern. Fan-beam elements have a repetitive triangular-shaped transmission pattern with zero transmissivity over half the pitch of 63″ along a direction. In this flare, we fortunately have two fan-beam elements to observe mainly the lower and higher coronal region as shown in Figure 3 (see fan-beam views). Using photon count rates obtained with these elements, we can derive spectral information of these two coronal regions even if we cannot discern any significant flux from the higher coronal sources in the lower energy bands.

Figure 5 shows the photon spectrum of these two regions derived from the fan-beam data. The assumed model to explain the observed count rates is a thermal (single temperature) plus a nonthermal (single power law) component as proposed by Sato & Hanaoka (2000). For the thermal component, it is clear that the temperature is very similar for both regions (except for the difference in the EMs) and that it is dominant in the L and M1 bands. The nonthermal component has the following characteristics: (1) The spectrum is hard in both regions, with the lower coronal region showing a harder spectrum than in the higher region. (2) In the higher coronal region, the component is dominant in the M2 band.

5. SUMMARY AND REMARKABLE POINTS

We observed several coronal hard X-ray sources during the 1998 April 23 flare. The hard X-ray sources observed in the M2 band are classified as three types. (1) There is a thermal source (N) in the northern region, which moves along the top

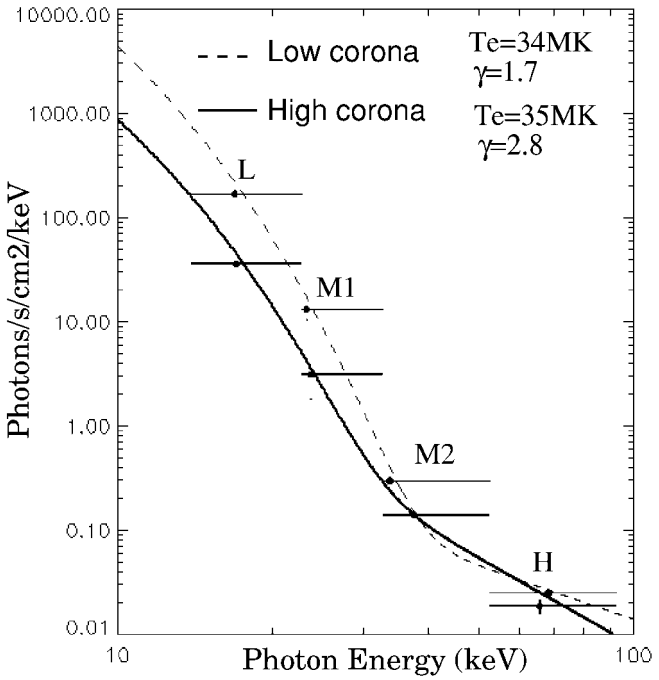

FIG. 5.—Hard X-ray spectra obtained from fan-beam data for the lower and higher coronal regions during the time interval g. The observing regions for the two fan-beam elements are shown in Fig. 3. The assumed spectra and the measured photon fluxes (*horizontal bars*) are plotted. Fitting is done between the observed counts and the counts expected from the assumed spectrum, and we achieved a reduced $\chi^2 = 1.0$ for both cases. The mean energy of the assumed spectrum in each band is shown as a vertical bar corresponding to a ± 1 σ error. γ and Te are the power-law index and electron temperature, respectively.

of the soft X-ray arcade during the impulsive phase. (2) There are nonthermal sources (S1 and S2) in the low corona. These are located above the top of the bright soft X-ray arcade structure in the southern region. S1 is visible during two spikes in the hard X-ray time profile. S2 shows a cusplike structure, and the centroid position moves into the higher corona temporarily around the hard X-ray peak time. (3) There is an extended source (E) located in the higher corona. This source shows gradual time variation and is delayed from the other nonthermal sources by about 2 minutes. It has a nonthermal component with a hard spectrum.

Strong thermal and nonthermal sources in the low corona must be made by different processes since they are not all at the same location except at the beginning of the event. Tomczak (1997) showed similar observational characteristics in a large-sized flare. In these events, most of the thermal plasma may be produced via heat conduction rather than by accelerated electrons. Also, the displacement between thermal and nonthermal sources may be a common phenomenon even in compact flares. Since the nonthermal sources observed in the low corona are located above the soft X-ray loops and are well observed in the impulsive phase, they may correspond to Masuda sources. Considering the effect of the line of sight of these sources observed at different loop-top regions, we can explain why some of Masuda's loop-top events are not observed outside the bright soft X-ray loop as described in Masuda et al. (1995).

No similar observation of an extended hard X-ray source has previously been reported, although a high coronal source was reported as a type C flare by Cliver et al. (1986). One of the well-known characteristics of type C flares is that the hard X-ray emission has a hard spectrum. The extended coronal source studied here has this characteristic. Our observations may suggest that a type C flare is not a single source but is composed of multiple sources at different altitudes in the corona.

These observations show that the low and high coronal nonthermal sources have common features such as a hard spectrum and a related evolution of spatial structures. The high coronal source shows a delayed peak, but the low coronal source is still strong at that time. This suggests that energetic phenomena occur in the low corona and then a part of the energetic electrons are injected into the high corona, although we do not have an explanation of the 2 minute delay. The Masuda source probably corresponds to the low coronal sources seen in this flare. It may be the origin of the high coronal source. Alternately, the reconnection site moves to higher loops, and a new episode of particle acceleration takes place over a large area and at a higher altitude.

High-quality imaging is one of the most important keys to understanding coronal hard X-ray sources. We look forward to analyzing HESSI observations of similar extended coronal sources using its superior imaging capability and spectral resolution.

Yohkoh is a mission of the Institute of Space and Astronautical Sciences, Japan, with multilateral international collaboration with NASA (US) and PPARC (UK). The author is grateful to B. R. Dennis for valuable comments. This work was finished while the author held a National Research Council Research Associateship at NASA's Goddard Space Flight Center.

REFERENCES

Alexander, D., & Metcalf, T. R. 1997, ApJ, 489, 442
Cliver, E. W., Dennis, B. R., Kiplinger, A. L., Kane, S. R., Neidig, D. F., Sheeley, N. R., Jr., & Koomen, M. J. 1986, ApJ, 305, 920
Kosugi T., et al. 1991, Sol. Phys., 136, 17
Masuda, S., Kosugi, T., Hara, H., Sakao, T., Shibata, K., & Tsuneta, S. 1995, PASJ, 47, 677
Sato, J., & Hanaoka, Y. 2000, in Proc. Nobeyama Symp., ed. A. Dalgarno (NRO Rep. 479; Nagano: NRO), 349
Sato, J., Kosugi, T., & Makishima, K. 1999, PASJ, 51, 127
Tomczak, M. 1997, A&A, 317, 223
Tsuneta, S., et al. 1991, Sol. Phys., 136, 37
Yoshimori, M., et al. 1991, Sol. Phys., 136, 69